Hindawi
Advances in High Energy Physics
Volume 2020, Article ID 5064737, 11 pages
https://doi.org/10.1155/2020/5064737

Research Article

Light Particle and Quark Chemical Potentials from Negatively to Positively Charged Particle Yield Ratios Corrected by Removing Strong and Weak Decays

Hai-Ling Lao,[1] Ya-Qin Gao ,[2] and Fu-Hu Liu [1]

[1]*Institute of Theoretical Physics and State Key Laboratory of Quantum Optics and Quantum Optics Devices, Shanxi University, Taiyuan 030006, Shanxi, China*
[2]*Department of Physics, Taiyuan University of Science and Technology, Taiyuan, Shanxi 030024, China*

Correspondence should be addressed to Fu-Hu Liu; fuhuliu@163.com

Received 1 June 2019; Revised 31 July 2019; Accepted 11 August 2019; Published 9 January 2020

Academic Editor: Antonio J. Accioly

The yield ratios of negatively to positively charged pions (π^-/π^+), negatively to positively charged kaons (K^-/K^+), and anti-protons to protons ($\overline{p}/p$) produced in mid-rapidity interval in central gold-gold (Au-Au) collisions, central lead-lead (Pb-Pb) collisions, and inelastic (INEL) or non-single-diffractive (NSD) proton-proton (pp) collisions, as well as in forward rapidity region in INEL pp collisions are analyzed in the present work. Over an energy range from a few GeV to above 10 TeV, the chemical potentials of light flavor particles (pion, kaon, and proton) and quarks (up, down, and strange quarks) are extracted from the mentioned yield ratios in which the contributions of strong decay from high-mass resonance and weak decay from heavy flavor hadrons are removed. Most energy dependent chemical potentials show the maximum at about 4 GeV, while the energy dependent yield ratios do not show such an extremum.

1. Introduction

The yield ratios of negatively to positively charged pions (π^-/π^+), negatively to positively charged kaons (K^-/K^+), and anti-protons to protons ($\overline{p}/p$), as well as the yield rations of other different particles are important quantities measured in experiments, where the symbol of a given particle is used for its yield for the purpose of simplicity. Based on the yield ratios, one can obtain the chemical freeze-out temperature (T_{ch}) of interacting system and the chemical potential (μ_{baryon}) of baryon in the framework of statistical thermal model [1–4]. In the phase diagram of quantum chromodynamics (QCD), T_{ch} and μ_{baryon} describe together the phase transition from hadronic matter to quark-gluon plasma (QGP) or quark matter [4–7]. Except for μ_{baryon}, the chemical potentials of light particles (pion, kaon, and proton) and light quarks (up, down, and strange quarks) are also interesting and important in the studies of system evolution and particle production.

According to the statistical thermal model [1–4], to study the chemical potentials of light particles and quarks, we need the yield ratios of π^-/π^+, K^-/K^+, and $\overline{p}/p$ at the stage of chemical freeze-out at which inelastic collisions stop. However, the data measured in experiments are usually at the stage of past chemical freeze-out or kinetic freeze-out at which the strong decay from high-mass resonance and weak decay from heavy flavor hadrons contribute to the yield ratios [8], where the kinetic freeze-out is a stage of system evolution at which the probability density functions of particle momenta are invariant. To use the expression of T_{ch} and to obtain the chemical potentials of light particles and quarks in the framework of statistical thermal model [1–4], one should remove the contributions of strong decay from high-mass resonance and weak decay from heavy flavor hadrons to the yield ratios of π^-/π^+, K^-/K^+, and $\overline{p}/p$ measured in experiments [8].

Presently, the yield ratios of π^-/π^+, K^-/K^+, and $\overline{p}/p$ produced in nucleus-nucleus and proton-proton (pp) collisions at high energies are available to collect [9] in experiments [6, 10–31]. Although the yield ratios in asymmetric collisions are also available, we analyze more simply the yield ratios in mid-rapidity interval in central gold-gold (Au-Au) collisions at the Alternating Gradient Synchrotron (AGS) and the Relativistic Heavy Ion Collider (RHIC) within its Beam

Energy Scan (BES) program, in central lead-lead (Pb-Pb) collisions at the Super Proton Synchrotron (SPS) and the Relativistic Heavy Ion Collider (RHIC), and in inelastic (INEL) or non-single-diffractive (NSD) proton-proton (pp) collisions at the SPS and the Large Hadron Collider (LHC), as well as in forward rapidity region in INEL pp collisions at the SPS at its BES. These data are measured by some international collaborations over a center-of-mass energy per nucleon pair ($\sqrt{s_{NN}}$) range from a few GeV to above 10 TeV [6, 10–31].

In this paper, we analyze the chemical potentials of light particles and quarks based on the yield ratios in the framework of statistical thermal model [1–4]. Comparing with our recent work [9], the contributions of strong decay from high-mass resonance and weak decay from heavy flavor hadrons to the yield ratios are removed. The energy dependent chemical potentials of light particles and quarks are obtained.

2. The Method and Formalism

To extract the chemical potentials of light particles and quarks, the yield ratios of π^-/π^+, K^-/K^+, and $\overline{p}/p$ produced in Au-Au (Pb-Pb) and pp collisions at the AGS, SPS at its BES, RHIC at its BES, and LHC are needed, where the contributions of strong and weak decays to the yield rations should be removed. The same formula on the relation between the yield ratio and chemical potential are used in our previous work [9, 32] and the present work due to the standard and unified expression. This results in some repetitions which are ineluctable to give a whole representation of the present work.

In the framework of statistical thermal model of noninteracting gas particles with the assumption of standard Boltzmann–Gibbs statistics [1–4], based on the Boltzmann approximation in the employ of grand-canonical ensemble, one has empirically [4, 5, 33–35]

$$T_{ch} = T_{\lim}\frac{1}{1+\exp\left[2.60-\ln\left(\sqrt{s_{NN}}\right)/0.45\right]}, \tag{1}$$

where $\sqrt{s_{NN}}$ is in units of GeV and the "limiting" temperature $T_{\lim} \approx 0.16$ GeV. Meanwhile, based on the Boltzmann approximation and the relation to isospin effect, one has the relation among $\overline{p}/p$, T_{ch}, and chemical potential μ_p of proton to be [17, 36, 37]

$$\frac{\overline{p}}{p} = \exp\left(-\frac{2\mu_p}{T_{ch}}\right) \approx \exp\left(-\frac{2\mu_{baryon}}{T_{ch}}\right). \tag{2}$$

Equations (1) and (2) are valid at the stage of chemical freeze-out which is earlier than the strong decay from high-mass resonance and weak decay from heavy flavor hadrons.

Similar to Equation (2), π^-/π^+, K^-/K^+, and other two negatively to positively charged particles (D^-/D^+ and B^-/B^+) with together $\overline{p}/p$ are uniformly shown to be

$$k_j \equiv \frac{j^-}{j^+} = \exp\left(-\frac{2\mu_j}{T_{ch}}\right), \tag{3}$$

where $j = \pi, K, p, D$, and B; k_j denote the yield ratio of negatively to positively charged particle j; and μ_j denote the chemical potential of the particle j.

To obtain chemical potentials of quarks, the five yield ratios, k_j ($j = \pi, K, p, D$, and B), are enough. We shall not discuss the yield ratio of top quark related antiparticles and particles, top quark itself, and chemical potentials of top quark related particle and top quark due to the fact that the lifetimes of particles contained top quark are very short to be measured.

The chemical potential for quark flavor q is denoted by μ_q, where $q = u, d, s, c$, and b represent the up, down, strange, charm, and bottom quarks, respectively. The values of μ_q are then expected due to Equation (3). According to Refs. [38, 39], k_j ($j = \pi, K, p, D$, and B) are expressed by T_{ch} and μ_q ($q = u, d, s, c$, and b) to be

$$\begin{aligned}
k_\pi &= \exp\left[-\frac{2\left(\mu_u-\mu_d\right)}{T_{ch}}\right],\\
k_K &= \exp\left[-\frac{2\left(\mu_u-\mu_s\right)}{T_{ch}}\right],\\
k_p &= \exp\left[-\frac{2\left(2\mu_u+\mu_d\right)}{T_{ch}}\right],\\
k_D &= \exp\left[-\frac{2\left(\mu_c-\mu_d\right)}{T_{ch}}\right],\\
k_B &= \exp\left[-\frac{2\left(\mu_u-\mu_b\right)}{T_{ch}}\right].
\end{aligned} \tag{4}$$

According to Equations (3) and (4), μ_j of particle j and μ_q of quark q can be obtained in terms of k_j or their combination to be

$$\mu_j = -\frac{1}{2}T_{ch}\ln k_j, \tag{5}$$

$$\begin{aligned}
\mu_u &= -\frac{1}{6}T_{ch}\left(\ln k_\pi + \ln k_p\right),\\
\mu_d &= -\frac{1}{6}T_{ch}\left(-2\ln k_\pi + \ln k_p\right),\\
\mu_s &= -\frac{1}{6}T_{ch}\left(\ln k_\pi - 3\ln k_K + \ln k_p\right),\\
\mu_c &= -\frac{1}{6}T_{ch}\left(-2\ln k_\pi + \ln k_p + 3\ln k_D\right),\\
\mu_b &= -\frac{1}{6}T_{ch}\left(\ln k_\pi + \ln k_p - 3\ln k_B\right),
\end{aligned} \tag{6}$$

respectively.

Although we show formula on D, B, c, and b in Equations (3)–(6), there is no k_D and k_B are analyzed in the present work due to the limited data. The expressions on D, B, c, and b have only significance in methodology. In fact, the present work focuses only k_j and μ_j of light flavor particles, π, K, and p, as well as μ_q of light flavor quarks, u, d, and s.

It should be noted that Equation (1) means a single-T_{ch} scenario for the chemical freeze-out. It is unambiguous that a two- or multi-T_{ch} scenario is also possible [40–44]. In the case of using the two-T_{ch}, we need $T_{ch,S}$ for strange particles and $T_{ch,NS}$ for nonstrange particles. Thus, Equations (3)–(6) are revised to

$$\begin{aligned}
k_K &\equiv \frac{K^-}{K^+} = \exp\left(-\frac{2\mu_K}{T_{ch,S}}\right),\\
k_j &\equiv \frac{j^-}{j^+} = \exp\left(-\frac{2\mu_j}{T_{ch,NS}}\right), \quad (j \neq K),
\end{aligned} \tag{7}$$

Table 1: The (pseudo)rapidity intervals, centrality ranges or collision types, and collision systems corresponding to the yield ratios quoted in Figure 1.

Open symbol	(Pseudo)rapidity	Centrality or Type	Collisions	Collaboration	Reference
Circles	$\|y\| < 0.05$ to $\|y\| < 0.4$	0–5%	Au-Au, AGS	E895, E866, E917	[10–12]
Squares	$\|y\| < 0.4$	0–10%	Au-Au, AGS	E802, E866	[13, 14]
Triangles	$\|\eta\| < 0.35$	0–5%	Au-Au, RHIC	PHENIX	[15–17]
Stars	$\|y\| < 0.1$ to $\|y\| < 0.5$	0–5% to 0–10%	Au-Au, RHIC	STAR	[6, 18–20]
Circles with +	$0 < y < 0.2$ or $\|y\| < 0.1$ to $\|y\| < 0.6$	0–5% to 0–7.2%	Pb-Pb, SPS	NA49	[21–24]
Squares with +	$\|y\| < 0.5$ to $\|y\| < 0.85$	0–3.7%	Pb-Pb, SPS	NA44	[25]
Triangles with +	$\|y\| < 0.5$	0–5%	Pb-Pb, LHC	ALICE	[26]
Circles with ×	$y > 0$	INEL	pp, SPS	NA61/SHINE	[27]
Squares with ×	$\|y\| < 0.1$	NSD	pp, RHIC	STAR	[6, 28]
Triangles with ×	$\|y\| < 0.5$	INEL	pp, LHC	ALICE	[29]
Stars with ×	$\|y\| < 1$	INEL	pp, LHC	CMS	[30, 31]

$$
\begin{aligned}
k_\pi &= \exp\left[-\frac{2(\mu_u-\mu_d)}{T_{ch,NS}}\right],\\
k_K &= \exp\left[-\frac{2(\mu_u-\mu_s)}{T_{ch,S}}\right],\\
k_p &= \exp\left[-\frac{2(2\mu_u+\mu_d)}{T_{ch,NS}}\right],\\
k_D &= \exp\left[-\frac{2(\mu_c-\mu_d)}{T_{ch,NS}}\right],\\
k_B &= \exp\left[-\frac{2(\mu_u-\mu_b)}{T_{ch,NS}}\right],
\end{aligned}
\tag{8}
$$

$$
\begin{aligned}
\mu_K &= -\frac{1}{2}T_{ch,S}\ln k_j,\\
\mu_j &= -\frac{1}{2}T_{ch,NS}\ln k_j, (j \neq K),
\end{aligned}
\tag{9}
$$

$$
\begin{aligned}
\mu_u &= -\frac{1}{6}T_{ch,NS}\left(\ln k_\pi + \ln k_p\right),\\
\mu_d &= -\frac{1}{6}T_{ch,NS}\left(-2\ln k_\pi + \ln k_p\right),\\
\mu_s &= -\frac{1}{6}\left(T_{ch,NS}\ln k_\pi - 3T_{ch,S}\ln k_K + T_{ch,NS}\ln k_p\right),\\
\mu_c &= -\frac{1}{6}T_{ch,NS}\left(-2\ln k_\pi + \ln k_p + 3\ln k_D\right),\\
\mu_b &= -\frac{1}{6}T_{ch,NS}\left(\ln k_\pi + \ln k_p - 3\ln k_B\right),
\end{aligned}
\tag{10}
$$

respectively.

The multi-T_{ch} scenario will result in different chemical freeze-out temperature $T_{ch,j}$ for emission of particles j^- and j^+. In the case of considering the multi-T_{ch} scenario, Equations (3)–(6) should be revised to

$$
k_j \equiv \frac{j^-}{j^+} = \exp\left(-\frac{2\mu_j}{T_{ch,j}}\right),
\tag{11}
$$

$$
\begin{aligned}
k_\pi &= \exp\left[-\frac{2(\mu_u-\mu_d)}{T_{ch,\pi}}\right],\\
k_K &= \exp\left[-\frac{2(\mu_u-\mu_s)}{T_{ch,K}}\right],\\
k_p &= \exp\left[-\frac{2(2\mu_u+\mu_d)}{T_{ch,p}}\right],\\
k_D &= \exp\left[-\frac{2(\mu_c-\mu_d)}{T_{ch,D}}\right],\\
k_B &= \exp\left[-\frac{2(\mu_u-\mu_b)}{T_{ch,B}}\right],
\end{aligned}
\tag{12}
$$

$$
\mu_j = -\frac{1}{2}T_{ch,j}\ln k_j,
\tag{13}
$$

$$
\begin{aligned}
\mu_u &= -\frac{1}{6}\left(T_{ch,\pi}\ln k_\pi + T_{ch,p}\ln k_p\right),\\
\mu_d &= -\frac{1}{6}\left(-2T_{ch,\pi}\ln k_\pi + T_{ch,p}\ln k_p\right),\\
\mu_s &= -\frac{1}{6}\left(T_{ch,\pi}\ln k_\pi - 3T_{ch,K}\ln k_K + T_{ch,p}\ln k_p\right),\\
\mu_c &= -\frac{1}{6}\left(-2T_{ch,\pi}\ln k_\pi + T_{ch,p}\ln k_p + 3T_{ch,D}\ln k_D\right),\\
\mu_b &= -\frac{1}{6}\left(T_{ch,\pi}\ln k_\pi + T_{ch,p}\ln k_p - 3T_{ch,B}\ln k_B\right),
\end{aligned}
\tag{14}
$$

respectively.

In the actual treatment in the present work, we shall use the single-T_{ch} scenario due to the fact that Equation (1) is available in literature [4, 5, 33, 34]. The two- or multi-T_{ch} scenario has only significance in methodology, though they are also possible [40–44].

3. Results and Discussion

Figures 1(a)–1(c) present respectively the yield ratios, k_π, k_K, and k_p, of negatively to positively charged particles produced

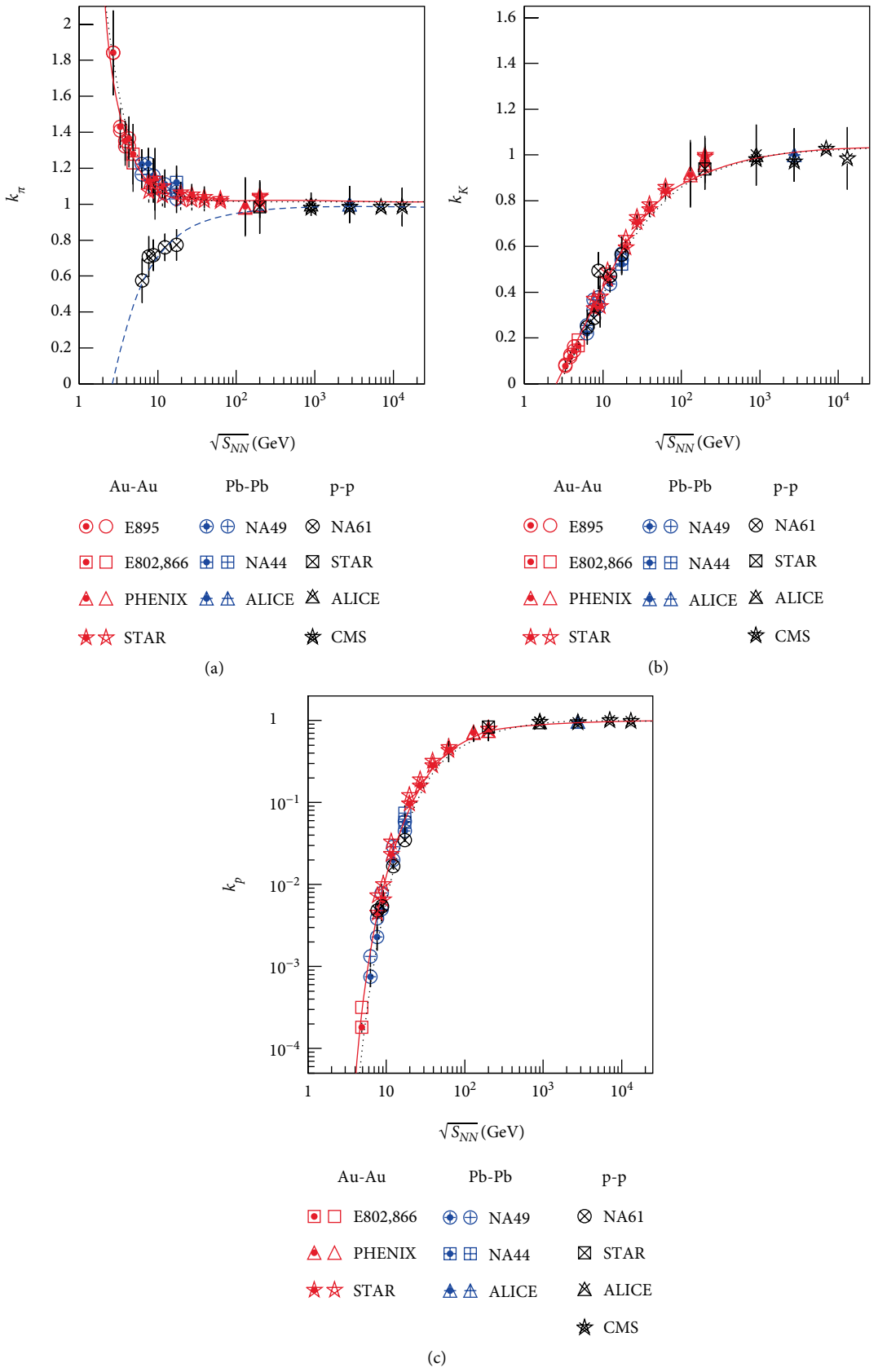

FIGURE 1: Yield ratios, (a) k_π, (b) k_K, and (c) k_p, of negatively to positively charged particles produced in mid-(pseudo)rapidity interval in central Au-Au collisions, central Pb-Pb collisions, and INEL or NSD pp collisions, as well as in forward rapidity region in INEL pp collisions. The circles, squares, triangles, and stars without •, or the symbols with + and without •, denote the yield ratios quoted in literature (see Table 1 for details). The circles, squares, triangles, and stars with •, or the symbols with + and •, denote the yield ratios corrected to the primary production by removing the contributions of strong decay from high-mass resonance and weak decay from heavy flavor hadrons [8]. The curves are the results fitted by us for the $\sqrt{s_{NN}}$ dependent k_j (see Equations (7)–(13) for details).

in mid-(pseudo)rapidity interval in central Au-Au collisions, central Pb-Pb collisions, and INEL or NSD pp collisions, as well as in forward rapidity region in INEL pp collisions. The circles, squares, triangles, and stars without •, or the symbols with + and without •, denote the yield ratios quoted in literature. The detailed (pseudo)rapidity intervals, centrality ranges or collision types, and collision systems are listed in Table 1 with together collaborations and references. The circles, squares, triangles, and stars with •, or the symbols with + and •, denote the yield ratios corrected to the primary production by removing the contributions of strong decay from high-mass resonance and weak decay from heavy flavor hadrons [8].

The solid (dotted) and dashed curves in Figure 1(a) are the results fitted by us for the $\sqrt{s_{NN}}$ dependent k_π in central Au-Au (Pb-Pb) collisions without (with) the corrections of decays and in INEL or NSD pp collisions respectively. The solid (dotted) curves in Figures 1(b) and 1(c) are the results fitted by us for the $\sqrt{s_{NN}}$ dependent k_K and k_p respectively, for the combining central Au-Au (Pb-Pb) collisions without (with) the corrections of decays and INEL or NSD pp collisions. One can see that, with the increase of $\sqrt{s_{NN}}$, k_π decreases obviously in central Au-Au (Pb-Pb) collisions and increases obviously in INEL or NSD pp collisions, and k_K and k_p increase obviously in both central Au-Au (Pb-Pb) and INEL or NSD pp collisions.

The solid, dotted, and dashed curves in Figure 1(a) can be empirically described by

$$k_\pi = (4.212 \pm 0.682) \cdot \left(\sqrt{s_{NN}}\right)^{-(1.799 \pm 0.152)} + (1.012 \pm 0.019), \quad (15)$$

$$k_\pi = (3.712 \pm 0.611) \cdot \left(\sqrt{s_{NN}}\right)^{-(1.519 \pm 0.148)} + (1.012 \pm 0.019), \quad (16)$$

$$k_\pi = -(2.453 \pm 0.292) \cdot \left(\sqrt{s_{NN}}\right)^{-(0.943 \pm 0.057)} + (0.984 \pm 0.009), \quad (17)$$

respectively, with χ^2/dof (χ^2 per degree of freedom) to be 0.162, 0.392, and 1.559 respectively. The solid and dotted curves in Figure 1(b) can be empirically described by

$$k_K = \left[-(0.291 \pm 0.028) + (0.306 \pm 0.010) \cdot \ln\left(\sqrt{s_{NN}}\right)\right] \cdot \theta\left(20 - \sqrt{s_{NN}}\right) + \left[-(2.172 \pm 0.146) \cdot \left(\sqrt{s_{NN}}\right)^{-(0.554 \pm 0.018)} + (1.039 \pm 0.016)\right] \cdot \theta\left(\sqrt{s_{NN}} - 20\right), \quad (18)$$

$$k_K = \left[-(0.299 \pm 0.029) + (0.299 \pm 0.009) \cdot \ln\left(\sqrt{s_{NN}}\right)\right] \cdot \theta\left(20 - \sqrt{s_{NN}}\right) + \left[-(2.372 \pm 0.146) \cdot \left(\sqrt{s_{NN}}\right)^{-(0.554 \pm 0.018)} + (1.039 \pm 0.016)\right] \cdot \theta\left(\sqrt{s_{NN}} - 20\right), \quad (19)$$

respectively, with χ^2/dof to be 2.735 and 2.355 respectively. The solid and dotted curves in Figure 1(c) can be empirically described by

$$k_p = \exp\left[-(34.803 \pm 3.685) \cdot \left(\sqrt{s_{NN}}\right)^{-(0.896 \pm 0.041)} - (0.008 \pm 0.004)\right] \quad (20)$$

$$k_p = \exp\left[-(37.403 \pm 3.776) \cdot \left(\sqrt{s_{NN}}\right)^{-(0.884 \pm 0.036)} - (0.007 \pm 0.003)\right] \quad (21)$$

respectively, with χ^2/dof to be 7.715 and 5.323, respectively.

The differences between the yield ratios without and with the corrections of decays appear mainly over an energy range from a few GeV to 100 GeV, though the differences are not very large. In particular, the difference seems to be the largest at about 10 GeV. The limiting values of all the three yield ratios are one at very high energy. According to the functions Equations (7)–(13), by using Equations (5) and (6), the chemical potentials, μ_π, μ_K, and μ_p, of light particles, π, K, and p, as well as the chemical potentials, μ_u, μ_d, and μ_s, of light quarks, u, d, and s, can be obtained respectively.

The $\sqrt{s_{NN}}$ dependent μ_π, $\mu_K\mu_p$ are shown in Figures 2(a)–2(c), respectively. The symbols denote the derivative data obtained from Figure 1 according to Equation (5), where different symbols correspond to different collaborations marked in the panels which are the same as Figure 1. Because of the chemical freeze-out temperature in pp collisions being unavailable, we use T_{ch}, $0.9T_{ch}$, and $0.8T_{ch}$ in Equation (5) to obtain the derivative data in INEL or NSD pp collisions, in which the corresponding results are orderly denoted by normal, medium, and small symbols with diagonal crosses. One can see that a low chemical freeze-out temperature in pp collisions results in low chemical potentials.

In Figure 2(a), the solid, dotted, and dashed curves represent the same data samples as Figure 1(a), but showing μ_π. In Figures 2(b) and 2(c), the solid and dotted curves represent the same data samples as Figures 1(a) and 1(c), but showing μ_K and μ_p respectively. One can see that, with the increase of $\sqrt{s_{NN}}$, μ_π increases and decreases obviously in central Au-Au (Pb-Pb) collisions and in INEL or NSD pp collisions respectively, while μ_K and μ_p decrease obviously in both central Au-Au (Pb-Pb) and INEL or NSD pp collisions. At very high energy, all of μ_π, μ_K, and μ_p approach to zero.

Figure 3 is the same as Figure 2, but Figures 3(a)–3(c) present respectively the $\sqrt{s_{NN}}$ dependent μ_u, μ_d, and μ_s, which are derived from the symbols and curves in Figure 1 according to Equation (6). The different symbols correspond to different collaborations marked in the panels which are the same as Figures 1 and 2. The solid (dotted) and dashed curves are for central Au-Au (Pb-Pb) collisions without (with) the corrections of decays and for INEL or NSD pp collisions respectively, One can see that, with the increase of $\sqrt{s_{NN}}$, μ_u, μ_d, and μ_s decrease obviously in both central Au-Au (Pb-Pb) and INEL or NSD pp collisions. Like μ_π, μ_K, and μ_p, all of μ_u, μ_d, and μ_s also approach to zero at very high energy.

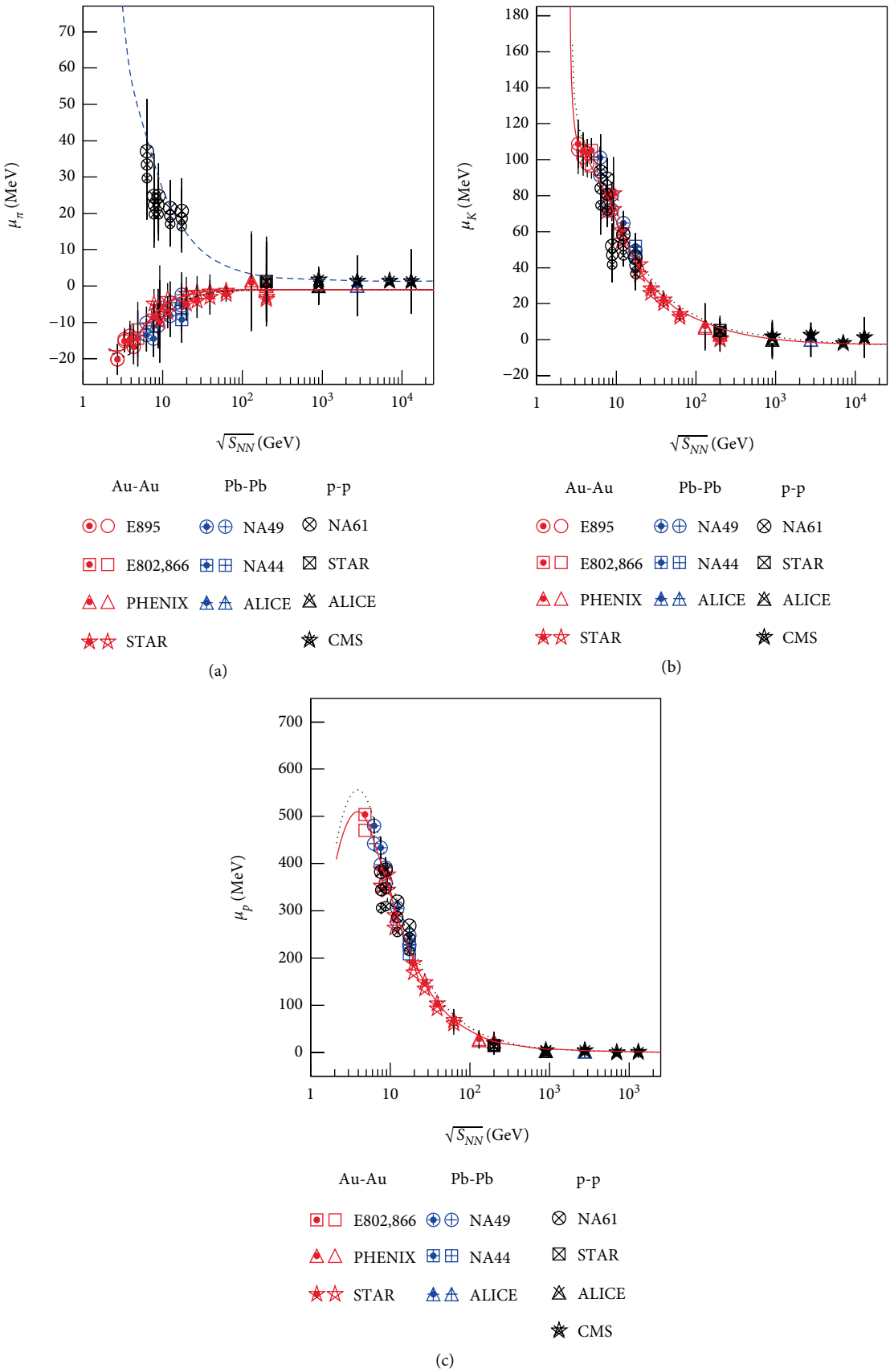

FIGURE 2: Chemical potentials, (a) μ_π, (b) μ_K, and (c) μ_p, of (a) π, (b) K, and (c) p produced in mid-(pseudo)rapidity interval in central Au-Au collisions, central Pb-Pb collisions, and INEL or NSD pp collisions, as well as in forward rapidity region in INEL pp collisions. The symbols denote the derivative data obtained from Figure 1 according to Equation (5). The normal, medium, and small symbols with diagonal crosses denote the derivative data in INEL or NSD pp collisions obtained by T_{ch}, $0.9T_{ch}$, and $0.8T_{ch}$ in Equation (5), respectively. The curves surrounded the symbols are the derivative results obtained from the curves in Figure 1 according to Equation (5).

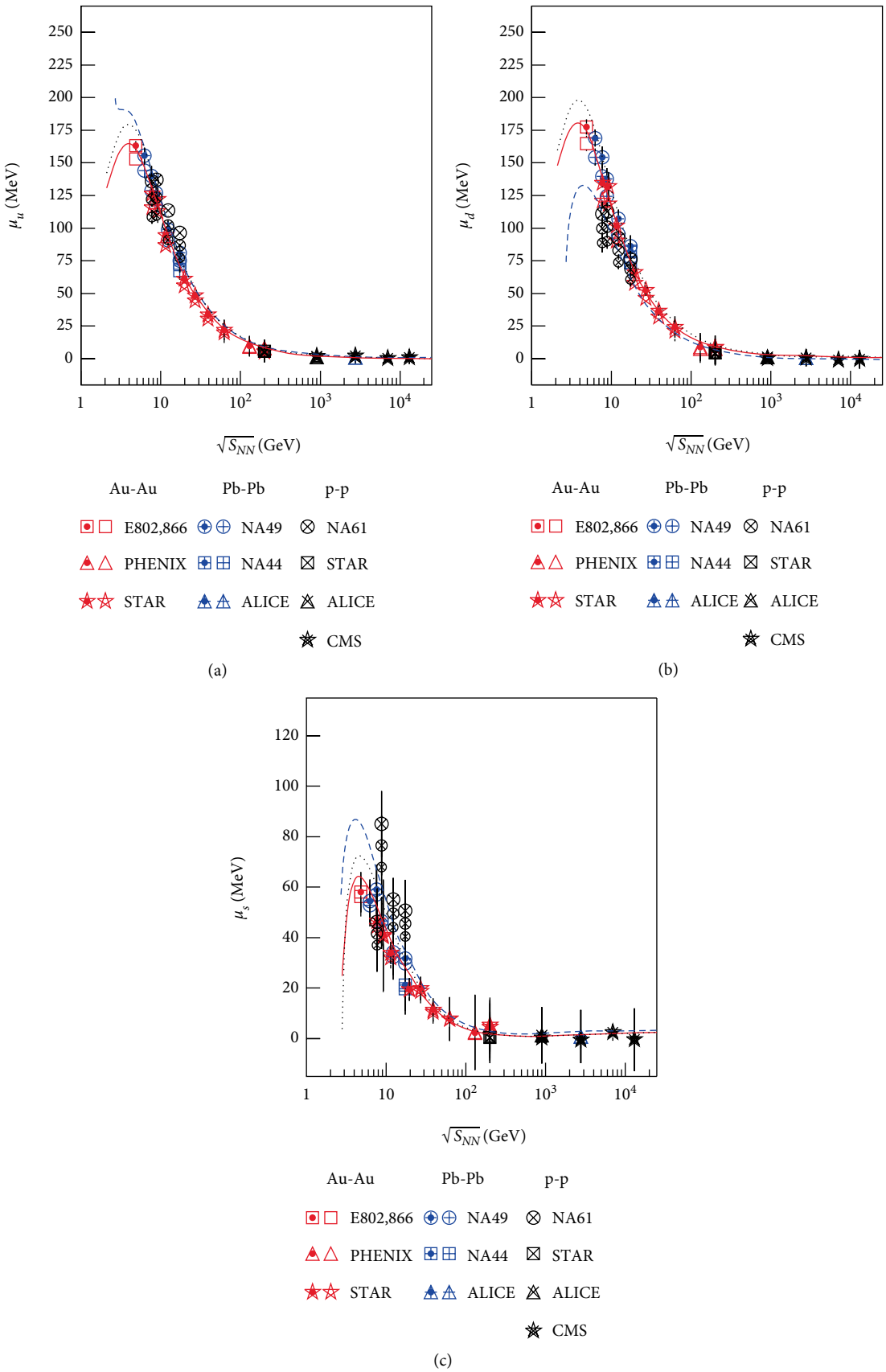

FIGURE 3: The same as Figure 2, but showing the chemical potentials, (a) μ_u, (b) μ_d, and (c) μ_s, of (a) u, (b) d, and (c) s quarks according to Equation (6). The solid (dotted) and dashed curves are for central Au-Au (Pb-Pb) collisions without (with) the corrections of decays and for INEL or NSD pp collisions respectively.

From Figures 1 to 3 one can see that, in central Au-Au (Pb-Pb) collisions, k_π (> 1) decreases obviously and k_K (< 1) and k_p (< 1) increase obviously with the increase of $\sqrt{s_{NN}}$. These differences also result in difference between μ_π and μ_K (μ_p). These differences are caused by different mechanisms in productions of pions, kaons, and protons. The contribution of strong and weak decays to k_π is larger than those to k_K and k_p. Comparing with pions, kaons have larger cross-section of absorbtion in nuclei. In the production of protons, the primary protons existed in the impact nuclei also affect the yield.

At the top RHIC (200 GeV) and LHC energies, the trends of k_j, μ_j, and μ_q in central Au-Au (Pb-Pb) collisions are close to those in INEL or NSD pp collisions due to the increase of hard scattering component. Finally, k_j approaches to one and μ_j and μ_q approaches to zero. These limiting values render that the hard scattering process contributes largely, the mean-free-path of produced particles (quarks) becomes largely, and the viscous effect becomes weakly at the LHC. Meanwhile, the interacting system changes completely from the hadron-dominant state to the quark-dominant state at the early and medium stage of collisions, though the final stage is hadron-dominant at the LHC.

The energy dependent μ_p, μ_u, μ_d, and μ_s also show the maximum at about 4 GeV, while the energy dependent μ_π, μ_K, k_π, k_K, and k_p do not show such an extremum. The particular trend of the considered curves are caused by some reasons. In terms of nuclear and hadronic fragmentation, over an energy range from MeV to GeV, impact nuclei undergone various modes of nuclear fission and fragmentation, as well as multi-fragmentation and limiting fragmentation, then hadronic fragmentation and limiting fragmentation appear. At the stage of nuclear limiting fragmentation [45], nuclear fragments have similar multiplicity and charge distributions. At the stage of hadronic limiting fragmentation, the (pseudo)rapidity spectra of relativistic produced particles in forward (backward) rapidity region have the same or similar shape [46]. For heavy nucleus such as Au and Pb, the initial energy of hadronic limiting fragmentation is possibly about 4 GeV. In terms of phase transition, about 4 GeV is possibly the initial energy of the phase transition from a liquid-like state of nucleons and mesons with a relatively short mean-free-path to a gas-like state of nucleons and mesons with a relatively long mean-free-path in central Au-Au (Pb-Pb) collisions.

Theoretically, chemical potentials always correspond to some conserved charge. In Ref. [34], it is written how a hadron j has a chemical potential μ_j. One has

$$\mu_j = \mu_{baryon} B_j + \mu_S S_j + \mu_I I_j + \mu_C C_j, \tag{22}$$

where B_j, S_j, I_j, and C_j are respectively the baryon number, strangeness, isospin, and charm of the considered particle j, and μ with lower foot marks $baryon$, S, I, and C correspond to respective chemical potentials. Not all of the four quantum numbers and four chemical potentials in the expression of μ_j are free parameters since some of them are fixed by the conservation laws and some of them are zero for a special particle.

Both Equations (5) and (22) are obtained in the framework of statistical thermal model [34, 36–39] or related literature [17]. These two formulas are different methods, but they should be harmonious in description of particle chemical potential at the stage of chemical freeze-out which is earlier than the strong and weak decays. Using Equation (5) with or without the corrections of strong and weak decays causes a small difference of particle chemical potentials. Using Equation (22) we have concretely $\mu_\pi = \mu_I I_\pi$, $\mu_K = \mu_S S_K + \mu_I I_K$, and $\mu_p = \mu_{baryon} B_p + \mu_I I_p$ which should give similar results to Equation (5) with or without the corrections of strong and weak decays. In particular, both Equations (5) and (22) results in zero chemical potential at above top RHIC energy. However, Equation (22) is not available to determine μ_q. Instead, the present work shows a way to determine μ_j and μ_q simultaneously.

To determine μ_j for a given particle j and μ_q for a given quark q, the present work has used a simple, convenient, and alternative method. In the case of utilizing T_{ch}, μ_j and μ_q can be obtained according to k_j which is obtained in experiments independently. Then, we can easily use Equation (5) for each particle independently and Equation (6) for each quark independently. In the extraction, we have neglected the difference between the chemical potential μ_{j^-} of negatively charged particle j^- and the chemical potential μ_{j^+} of positively charged particle j^+ due to small difference between μ_{j^-} and μ_{j^+}. Meanwhile, we have neglected the difference between the chemical potential $\mu_{\overline{q}}$ of anti-quark $\overline{q}$ and the chemical potential μ_q of quark q due to small difference between $\mu_{\overline{q}}$ and μ_q. Based on the above approximate treatment, Equations (1), (3), and (4) are acceptable. Besides, we have used a single-T_{ch} scenario for the chemical freeze-out, though a two-T_{ch} or multi-T_{ch} scenario is also possible.

Before summary and conclusions, it should be noted that although the contributions of strong decay from high-mass resonance and weak decay from heavy flavor hadrons [8] are excluded in the present work, only one mode of decay affects mainly k_π, k_K, or k_p measured in experiments. For k_π, removing the contribution of strong decay can regain the data from the stage at primary production, where the strong decay pulls down k_π. For k_K, removing the contribution of strong decay can regain the data from the stage at primary production, where the strong decay lifts k_K. For k_p, removing the weak decay can regain the data from the stage at primary production, where the weak decay lifts k_p. Generally, both strong and weak decays do not affect largely the trends of experimental k_j and then μ_j and μ_q, in particular at above top RHIC energy.

In the calculation on removing the contributions from strong and weak decays from the data, we have utilized a very recent literature [8] which works in the framework of statistical thermal model [1–4]. In ref. [8], the energy dependent particle ratios "from the stage at primary production, after strong decay from high-mass resonance, and after weak decay from heavy flavor hadrons" are presented. To compare with the data, the statistical thermal model [1–4, 8] is coordinately accounted the effects of experimental acceptance and transverse momentum cuts. What we do in the present work is to directly quote the results obtained in Ref. [8]. One can see that strong decay affects mainly k_π and k_K, while weak decay affects mainly k_p. Meanwhile, the effect of quantum statistics is much smaller and can be neglected [8].

In the case of including the contributions of two decays and quantum statistics [8], the extracted energy dependent μ_j

and μ_q have small difference from those excluding the mentioned contributions. Although the contributions of two decays to yields of π^- and π^+ are considerable, these effects to k_π are small. Except for the contributions to yields and yield ratios, the two decays also contribute mainly in low transverse momentum region and central rapidity interval. These contributions affect more or less the trends of transverse momentum and rapidity spectra in terms of slope or shape and normalization constant. We shall not discuss the effects of two decays on transverse momentum and rapidity spectra due to these topics being beyond the focus of the present work.

4. Summary and Conclusions

In summary, we have analyzed the yield ratios k_π, k_K, and k_p of negatively to positively charged particles produced in mid-(pseudo)rapidity interval in central Au-Au collisions, central Pb-Pb collisions, and INEL or NSD pp collisions, as well as in forward rapidity region in INEL pp collisions over a $\sqrt{s_{NN}}$ range from a few GeV to above 10 TeV. To obtain the chemical potentials μ_j and μ_q, k_π, k_K, and k_p are corrected by removing the contributions of strong decay from high-mass resonance and weak decay from heavy flavor hadrons. It is shown that, with the increase of $\sqrt{s_{NN}}$, k_π (> 1) decreases obviously in central Au-Au (Pb-Pb) collisions, k_π (< 1) increases obviously in INEL or NSD pp collisions, and k_K (< 1) and k_p (< 1) increase obviously in both central Au-Au (Pb-Pb) and INEL or NSD pp collisions. The limiting values of k_π, k_K, and k_p are one at very high energy.

The chemical potentials μ_π, μ_K, and μ_p of light particles π, K, and p, as well as the chemical potentials μ_u, μ_d, and μ_s of light quarks u, d, and s are extracted from the corrected yield ratios in which there is no contributions of two decays. With the increase of $\sqrt{s_{NN}}$ over a range from above a few GeV to above 10 TeV, μ_π (< 0) increases obviously in central Au-Au (Pb-Pb) collisions, μ_π (> 0) decreases obviously in INEL or NSD pp collisions, and μ_K (> 0) and μ_p (> 0) decrease obviously in both central Au-Au (Pb-Pb) and INEL or NSD pp collisions. Meanwhile, μ_u (> 0), μ_d (> 0), and μ_s (> 0) decrease obviously in both central Au-Au (Pb-Pb) and INEL or NSD pp collisions. The limiting values of μ_π, μ_K, μ_p, μ_u, μ_d, and μ_s are zero at very high energy. The difference between the results with and without the correction of two decays is not too large.

Even though for that with the corrections of two decays, the same particular energy is still existent as that without the corrections. The energy dependent μ_p, μ_u, μ_d, and μ_s show the maximum at about 4 GeV, while the energy dependent μ_π, μ_K, k_π, k_K, and k_p do not show such an extremum. For heavy nucleus such as Au and Pb, the initial energy of limiting fragmentation is possibly about 4 GeV. This energy is also possibly the initial energy of the phase transition from a liquid-like state of nucleons and mesons with a relatively short mean-free-path to a gas-like state of nucleons and mesons with a relatively long mean-free-path in central Au-Au (Pb-Pb) collisions. Meanwhile, the density of baryon number in nucleus-nucleus collisions at this energy has a large value. These particular factors render different trends of the considered quantities at this energy.

Data Availability

The data used to support the findings of this study are included within the article and are cited at relevant places within the text as references.

Ethical Approval

The authors declare that they are in compliance with ethical standards regarding the content of this paper.

Conflicts of Interest

The authors declare that they have no conflicts of interest.

Acknowledgments

This work was supported by the National Natural Science Foundation of China under Grant Nos. 11575103, 11847311, and 11747063, the Scientific and Technological Innovation Programs of Higher Education Institutions in Shanxi (STIP) under Grant No. 201802017, the Shanxi Provincial Natural Science Foundation under Grant No. 201701D121005, the Fund for Shanxi "1331 Project" Key Subjects Construction, and the Doctoral Scientific Research Foundation of Taiyuan University of Science and Technology under Grant No. 20152043. The funders had no role in the design of the study; in the collection, analyses, or interpretation of the data; in the writing of the manuscript, or in the decision to publish the results.

References

[1] J. Cleymans, B. Kämpfer, and S. Wheaton, "Centrality dependence of thermal parameters in heavy-ion collisions at relativistic energies," *Physical Review C*, vol. 65, Article ID 027901, 2002.

[2] F. Becattini, J. Manninen, and M. Gaździcki, "Energy and system size dependence of chemical freeze-out in relativistic nuclear collisions," *Physical Review C*, vol. 73, Article ID 044905, 2006.

[3] A. Andronic, P. Braun-Munzinger, K. Redlich, and J. Stachel, "Statistical hadronization of heavy quarks in ultra-relativistic nucleus-nucleus collisions," *Nuclear Physics A*, vol. 789, pp. 334–356, 2007.

[4] J. Cleymans, H. Oeschler, K. Redlich, and S. Wheaton, "Comparison of chemical freeze-out criteria in heavy-ion collisions," *Physical Review C*, vol. 73, Article ID 034905, 2006.

[5] A. Andronic, P. Braun-Munzinger, and J. Stachel, "The horn, the hadron mass spectrum and the QCD phase diagram: the statistical model of hadron production in central nucleus-nucleus collisions," *Nuclear Physics A*, vol. 834, pp. 237c–240c, 2010.

[6] L. Adamczyk, J. K. Adkins, G. Agakishiev et al., "Bulk properties of the medium produced in relativistic heavy-ion collisions from the beam energy scan program," *Physical Review C*, vol. 96, Article ID 044904, 2017.

[7] R. Bellwied, "Sequential strangeness freeze-out," *EPJ Web of Conferences*, vol. 171, p. 02006, 2018.

[8] N. Yu and X. Luo, "Particle decay from statistical thermal model in high-energy nucleus-nucleus collisions," *The European Physical Journal A*, vol. 55, p. 26, 2019.

[9] H.-L. Lao, Y.-Q. Gao, and F.-H. Liu, "Energy dependent chemical potentials of light particles and quarks from yield ratios of antiparticles to particles in high energy collisions," *Universe*, vol. 5, p. 152, 2019.

[10] J. L. Klay, N. N. Ajitanand, J. M. Alexander et al., "Charged pion production in 2A to 8A GeV central Au+Au collisions," *Physical Review C*, vol. 68, Article ID 054905, 2003.

[11] L. Ahle, Y. Akiba, K. Ashktorab et al., "An excitation function of K^- and K^+ production in Au+Au reactions at the AGS," *Physics Letters B*, vol. 490, pp. 53–60, 2000.

[12] J. L. Klay, N. N. Ajitanand, J. M. Alexander et al., "Longitudinal flow from (2–8)A GeV Au+Au collisions," *Physical Review Letters*, vol. 88, Article ID 102301, 2002.

[13] Y. Akiba, D. Alburger, D. Beavis et al., "Particle production in Au + Au collisions from BNL E866," *Nuclear Physics A*, vol. 610, pp. 139c–152c, 1996.

[14] L. Ahle, Y. Akiba, K. Ashktorab et al., "Particle production at high baryon density in central Au+Au reactions at 11.6A GeV/c," *Physical Review C*, vol. 57, pp. 466(R)–477(R), 1998.

[15] K. Adcox, S. S. Adler, N. N. Ajitanand et al., "Single identified hadron spectra from $\sqrt{s_{NN}} = 130$ GeV Au+Au collisions," *Physical Review C*, vol. 69, Article ID 024904, 2004.

[16] K. Adcox, S. S. Adler, N. N. Ajitanand et al., "Centrality dependence of π+/π-, K+/K-, p and p production from $\sqrt{s_{NN}} = 130$ GeV Au+Au collisions at RHIC," *Physical Review Letters*, vol. 88, Article ID 242301, 2002.

[17] S. S. Adler, S. Afanasiev, C. Aidala et al., "Identified charged particle spectra and yields in Au+Au collisions at $\sqrt{s_{NN}} = 200$ GeV," *Physical Review C*, vol. 69, Article ID 034909, 2004.

[18] B. I. Abelev, M. M. Aggarwal, Z. Ahammed et al., "Identified particle production, azimuthal anisotropy, and interferometry measurements in Au+Au collisions at $\sqrt{s_{NN}} = 9.2$ GeV," *Physical Review C*, vol. 81, Article ID 024911, 2010.

[19] B. I. Abelev, M. M. Aggarwal, Z. Ahammed et al., "Systematic measurements of identified particle spectra in pp, d+Au and Au+Au collisions from STAR," *Physical Review C*, vol. 79, Article ID 034909, 2009.

[20] J. Adams, C. Adler, M. M. Aggarwal et al., "Identified particle distributions in pp and Au+Au collisions at $\sqrt{s_{NN}} = 200$," *Physical Review Letters*, vol. 92, Article ID 112301, 2004.

[21] C. Alt, T. Anticic, B. Baatar et al., "Pion and kaon production in central Pb+Pb collisions at 20A and 30A GeV: evidence for the onset of deconfinement," *Physical Review C*, vol. 77, Article ID 024903, 2008.

[22] S. V. Afanasiev, T. Anticic, D. Barna et al., "Energy dependence of pion and kaon production in central Pb+Pb collisions," *Physical Review C*, vol. 66, Article ID 054902, 2002.

[23] C. Alt, T. Anticic, B. Baatar et al., "Energy and centrality dependence of $\overline{p}$ and p production and the $\overline{\Lambda}/\overline{p}$ ratio in Pb+Pb collisions between 20A GeV and 158A GeV," *Physical Review C*, vol. 73, Article ID 044910, 2006.

[24] S. V. Afanasiev, T. Anticic, B. Baatar et al., "Energy and centrality dependence of deuteron and proton production in Pb+Pb collisions at relativistic energies," *Physical Review C*, vol. 69, Article ID 024902, 2004.

[25] I. G. Bearden, H. Bøggild, J. Boissevain et al., "Particle production in central Pb+Pb collisions at 158A GeV/c," *Physical Review C*, vol. 66, Article ID 044907, 2002.

[26] B. Abelev, J. Adam, D. Adamova et al., "Centrality dependence of π, K, p production in Pb-Pb collisions at $\sqrt{s_{NN}} = 2.76$ TeV," *Physical Review C*, vol. 88, Article ID 044910, 2013.

[27] A. Aduszkiewicz, Y. Ali, E. Andronov et al., "Measurements of $\pi^{\pm}$, $K^{\pm}$, p and $\overline{p}$ spectra in proton-proton interactions at 20, 31, 40, 80 and 158 GeV/c with the NA61/SHINE spectrometer at the CERN SPS," *The European Physical Journal C*, vol. 77, p. 671, 2017.

[28] B. I. Abelev, J. Adams, M. M. Aggarwal et al., "Strange particle production in p+p collisions at $\sqrt{s} = 200$ GeV," *Physical Review C*, vol. 75, Article ID 064901, 2007.

[29] K. Aamodt, N. Abel, U. Abeysekara et al., "Production of pions, kaons and protons in pp collisions at $\sqrt{s} = 900$ GeV with ALICE at the LHC," *The European Physical Journal C*, vol. 71, p. 1655, 2011.

[30] S. Chatrchyan, V. Khachatryan, A. Sirunyan et al., "Study of the inclusive production of charged pions, kaons, and protons in pp collisions at $\sqrt{s} = 0.9$, 2.76, and 7 TeV," *The European Physical Journal C*, vol. 72, p. 2164, 2012.

[31] A. M. Sirunyan, A. Tumasyan, W. Adam et al., "Measurement of charged pion, kaon, and proton production in proton-proton collisions at $\sqrt{s} = 13$ TeV," *Physical Review D*, vol. 96, Article ID 112003, 2017.

[32] Y.-Q. Gao, H.-L. Lao, and F.-H. Liu, "Chemical potentials of light flavor quarks from yield ratios of negative to positive particles in Au+Au collisions at RHIC," *Advances in High Energy Physics*, vol. 2018, Article ID 6047960, 7 pages, 2018.

[33] A. Andronic, P. Braun-Munzinger, and J. Stachel, "Thermal hadron production in relativistic nuclear collision," *Acta Physica Polonica B*, vol. 40, pp. 1005–1012, 2009.

[34] A. Andronic, P. Braun-Munzinger, and J. Stachel, "Hadron production in central nucleus-nucleus collisions at chemical freeze-out," *Nuclear Physics A*, vol. 772, pp. 167–199, 2006.

[35] A. Andronic, P. Braun-Munzinger, K. Redlich, and J. Stachel, "Decoding the phase structure of QCD via particle production at high energy," *Nature*, vol. 561, pp. 321–330, 2018.

[36] P. Koch, J. Rafelski, and W. Greiner, "Strange hadron in hot nuclear matter," *Physics Letters B*, vol. 123, pp. 151–154, 1983.

[37] P. Braun-Munzinger, D. Magestro, K. Redlich, and J. Stachel, "Hadron production in Au-Au collisions at RHIC," *Physics Letters B*, vol. 518, pp. 41–46, 2001.

[38] I. Arsene, I. G. Bearden, D. Beavis et al., "Quark–gluon plasma and color glass condensate at RHIC? The perspective from the BRAHMS experiment," *Nuclear Physics A*, vol. 757, pp. 1–27, 2005.

[39] H. Zhao and F.-H. Liu, "On extraction of chemical potentials of quarks from particle transverse momentum spectra in high energy collisions," *Advances in High Energy Physics*, vol. 2015, Article ID 137058, 9 pages, 2015.

[40] S. Chatterjee, S. Das, L. Kumar et al., "Freeze-out parameters in heavy-ion collisions at AGS, SPS, RHIC, and LHC energies," *Advances in High Energy Physics*, vol. 2015, Article ID 349013, 20 pages, 2015.

[41] S. Chatterjee, B. Mohanty, and R. Singh, "Freezeout hypersurface at energies available at the CERN Large Hadron Collider from particle spectra: Flavor and centrality dependence," *Physical Review C*, vol. 92, 2015.

[42] S. Chatterjee and B. Mohanty, "Production of light nuclei in heavy-ion collisions within a multiple-freezeout scenario," *Physical Review C*, vol. 90, 2014.

[43] D. Thakur, S. Tripathy, P. Garg, R. Sahoo, and J. Cleymans, "Indication of a differential freeze-out in proton-proton and heavy-ion collisions at RHIC and LHC energies," *Advances in High Energy Physics*, vol. 2016, Article ID 4149352, 13 pages, 2016.

[44] H.-L. Lao, H.-R. Wei, F.-H. Liu, and R. A. Lacey, "An evidence of mass-dependent differential kinetic freeze-out scenario observed in Pb-Pb collisions at 2.76 TeV," *The European Physical Journal A*, vol. 52, p. 203, 2016.

[45] O. Lindfors, "Introduction to Joint Institute for Nuclear Research Dubna," USSR, 1980.

[46] M. I. Adamovich, M. M. Aggarwal, R. Arora et al., "Limiting fragmentation in oxygen-induced emulsion interactions at 14.6, 60, and 200 GeV/nucleon," *Physical Review Letters*, vol. 62, pp. 2801–2804, 1989.